

A Tire Temperature Adaptive Extended Kalman Filter for Sideslip Angle Estimation: Experimental Validation on a Race Track

Original

A Tire Temperature Adaptive Extended Kalman Filter for Sideslip Angle Estimation: Experimental Validation on a Race Track / Masoero, Andrea; Manca, Raffaele; Castellanos Molina, Luis M.; Tonoli, Andrea. - In: APPLIED SCIENCES. - ISSN 2076-3417. - 16:1(2026). [10.3390/app16010310]

Availability:

This version is available at: 11583/3007770 since: 2026-02-19T10:04:43Z

Publisher:

MDPI (Multidisciplinary Digital Publishing Institute)

Published

DOI:10.3390/app16010310

Terms of use:




This article is made available under terms and conditions as specified in the corresponding bibliographic description in the repository

Publisher copyright

(Article begins on next page)

Article

A Tire Temperature Adaptive Extended Kalman Filter for Sideslip Angle Estimation: Experimental Validation on a Race Track

Andrea Masoero, Raffaele Manca , Luis M. Castellanos Molina *  and Andrea Tonoli 

Center for Automotive Research and Sustainable Mobility, Mechatronics Laboratory, Department of Mechanical and Aerospace Engineering, Politecnico di Torino, Corso Duca degli Abruzzi, 24, 10129 Turin, Italy; s317402@studenti.polito.it (A.M.); raffaele.manca@polito.it (R.M.); andrea.tonoli@polito.it (A.T.)

* Correspondence: luis.castellanos@polito.it

Abstract

Real-time estimation of vehicle sideslip angle is essential for both safety and performance applications. This study presents a temperature-adaptive Extended Kalman Filter (EKF) that estimates the sideslip angle of a racing vehicle by integrating dynamic and kinematic information. A temperature-dependent Pacejka tire model, derived directly from track tests, is embedded in a 3-degree-of-freedom dual-track vehicle model and used within the EKF to compensate for temperature-induced variations in tire behavior. The adaptive model parameters are identified from standard on-track maneuvers conducted at different tire temperatures, without the need for additional indoor rig testing. Experimental validation on a race track demonstrates that incorporating tire temperature adaptation and combining dynamic and kinematic estimation significantly enhance estimation accuracy, particularly under low-grip and high-performance driving conditions attested by a reduction of 40–50% in RMS error and a further reduction in maximum absolute error.

Keywords: electric vehicle; slip angle estimation; Kalman filter; thermal tire model; magic formula; vehicle dynamics

1. Introduction

Accurate real-time estimation of the vehicle sideslip angle is essential for both active safety systems and performance-oriented control, particularly for yaw stability management [1]. Direct measurement of this variable typically requires either dual-antenna GPS systems or non-contact optical sensors. The former can provide the velocity of two points on the vehicle chassis to reconstruct the overall velocity vector and sideslip angle, but it suffers from packaging constraints and low sampling rates (typically 1 Hz), which are insufficient for dynamic estimation. Optical sensors, on the other hand, employ high-frequency cameras to detect the vehicle's ground speed and direction with excellent precision, but they are expensive and must be installed with a clear and unobstructed view of the road surface—posing integration challenges, especially for compact vehicles.

Given the limitations of direct measurement systems, observer-based and sensor-fusion estimation methods have been widely investigated, including inertial-based observers [2], inertial-GPS fusion approaches [3], and optimization-based constrained estimation frameworks [4]. Ref. [5] provides the optimal filtering formulations for several model-based vehicle state observers. These works have explored both kinematic and model-based approaches, and in some cases, adaptive schemes that account for variations in tire working



Academic Editor: Suchao Xie

Received: 24 November 2025

Revised: 20 December 2025

Accepted: 25 December 2025

Published: 28 December 2025

Copyright: © 2025 by the authors.

Licensee MDPI, Basel, Switzerland.

This article is an open access article distributed under the terms and

conditions of the [Creative Commons](https://creativecommons.org/licenses/by/4.0/)

[Attribution \(CC BY\)](https://creativecommons.org/licenses/by/4.0/) license.

conditions such as pressure, temperature, and wear [6]. The main objective of these efforts has been to develop robust and accurate sideslip estimation methods suitable for a wide range of driving scenarios. For instance, refs. [2,7] proposed a combined approach integrating dynamic estimation with a kinematic sideslip derivative. This pseudo-integration strategy improves robustness to modeling uncertainties, although the underlying dynamic model assumes a linear relation between tire lateral force and slip angle, leading to grip overestimation. Furthermore, their validation was limited to lateral maneuvers, without evaluating behavior at the limits of adhesion.

Unmodeled effects such as road conditions, tire parameter uncertainty, and parameter drift can significantly degrade estimation accuracy and the performance of model-based control systems. Jonathan et al. [8] showed that tire temperature and wear effects introduce significant variability in observed vehicle behavior during automated drifting maneuvers using nonlinear model predictive control (NMPC). Similarly, Kobayashi et al. [9] introduced a tire model that explicitly accounts for the temperature dependence of tire–road friction by incorporating a temperature state dynamic into vehicle trajectory planning, and validated its impact on automated drifting control performance through LQR-based experiments on a full-scale platform.

As highlighted in the review [10], several adaptive strategies have been proposed to address these issues through online tire-parameter updating for vehicle dynamics state estimation applications. Ahangarnejad et al. [11] employ a dual-EKF architecture to jointly estimate vehicle states and tire parameters, while Naets et al. [12] propose a two-stage estimator that performs online identification of tire model parameters.

In [6], an adaptive tire model and a UKF-based axle force observer were introduced to estimate sideslip angle. However, this method relies on extensive indoor tire testing, which is costly and difficult to replicate under real driving conditions. The model also considers only pure lateral tire dynamics, limiting its applicability when combined longitudinal and lateral forces occur.

To overcome these limitations, this work presents a temperature-adaptive sideslip angle estimation strategy that combines the strengths of kinematic and model-based approaches within an Extended Kalman Filter (EKF) framework. The proposed method dynamically adjusts the internal tire model using a temperature-adaptive Pacejka formulation derived directly from on-track experiments. Starting from a baseline .tir file, the Pacejka parameters are rescaled using data from standard track maneuvers performed at different tire temperatures, thus avoiding the need for additional laboratory testing.

The remainder of this paper is organized as follows. Section 2 introduces the case study vehicle, the experimental setup, and the test procedures. Section 3 describes the sideslip angle estimation algorithm, emphasizing the Extended Kalman Filter (EKF) architecture, the kinematic contribution, and the temperature-adaptive Pacejka tire model. Section 4 presents the experimental validation, including both pure lateral maneuvers and a complete track lap. The numerical results are analyzed and discussed in Section 5, focusing on estimation accuracy through RMS error, and Maximum Absolute Error metrics. Finally, Section 6 summarizes the main findings and outlines directions for future work.

2. Case Study Vehicle and Equipment

This study was conducted using an FSAE vehicle, shown in Figure 1, instrumented with several sensors for data acquisition during on-track testing and validation. The main measurements were provided by an IMU–GNSS N-Ellipse unit from SBG Systems [13], which supplied yaw rate (r) as well as lateral and longitudinal accelerations (a_y and a_x) with a sampling frequency of 200 Hz. Ground speed components (V_x and V_y) were measured using a Correvit S-Motion non-contact optical sensor from KISTLER (Winterthur, Switzer-

land) [14] with a sampling frequency of 500 Hz. From these quantities, the total speed magnitude (V) and vehicle slip angle (β) were derived. The lateral speed component was corrected to account for the distance between the vehicle's center of gravity (CoG) and the sensor position, as well as the measured yaw rate. The steering wheel angle (δ) was measured using an RM08 rotary magnetic encoder from RLS (Lake Mary, FL, USA) [15], a compact and high-speed sensor specifically designed for dynamic applications with a sampling frequency of 100 Hz. Temperature acquisitions are performed with a needle probe pyrometer HPM5 by Prisma Electronics (Pineto, TE, Italy), with an accuracy of ± 0.1 °C. All track tests were carried out using the FSAE vehicle, whose main characteristics are summarized in Table 1.

Table 1. Squadra Corse PoliTo FSAE vehicle data.

Parameter	Value	Unit
Mass without driver	207	kg
Front mass repartition	45	%
Wheelbase	1.525	m
Track width	1.202	m
Center of gravity height from ground	0.28	m
Suspension roll gradient	0.5	deg/g
Tires	185/40 R14 slick	–
Aerodynamic lift coefficient (C_L)	4.8	–
Aerodynamic drag coefficient (C_D)	1.5	–
Front aerodynamic balance	58	%
Acceleration (0–100 km/h)	2.6	s
Maximum speed	122	km/h
Maximum lateral acceleration	2.5	g
Powertrain type	Electric 4WD	–
Maximum motor power (data sheet)	35	kW

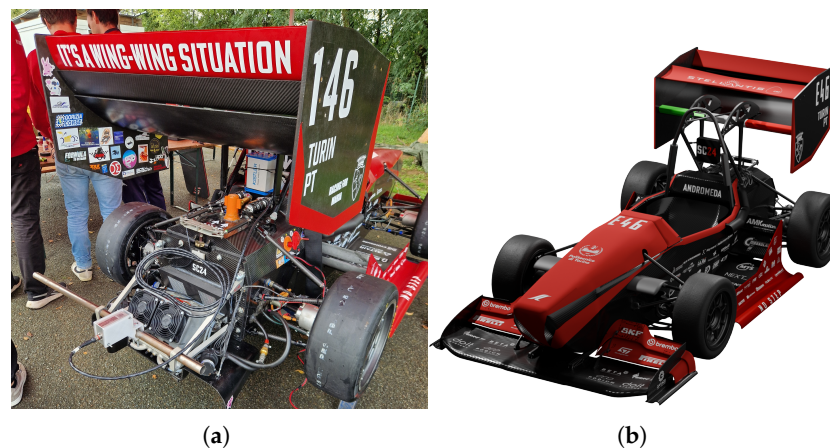


Figure 1. Relevant equipment for track tests: (a) Correvit S-Motion non-contact optical sensor mounted at the back of the vehicle, employed to measure the magnitude of vehicle speed and slip angle; (b) test vehicle.

The test campaign comprised several maneuvers designed to evaluate the vehicle dynamics and estimator performance under different conditions. The Double Lane Change (DLC) test, adapted from the standard automotive procedure, was executed at full throttle with the vehicle power limited to 12 kW, resulting in an entry speed of approximately 50 km/h. A Slalom maneuver with cone spacing of about 8 m was performed, during which the driver was instructed to brake at the entry gate and accelerate at the exit. The Constant Radius Cornering (CRC) test was conducted on a circular path with a radius of 10 m

to characterize tire behavior and to identify the required parameters, while a Steering Sine Sweep maneuver was carried out at various speeds to validate slip angle estimation. Finally, a complete Track Lap was performed on the test circuit, approximately 350 m in length, featuring tight corners and a maximum speed of around 80 km/h, with an average lap time of about 30 s. This test was used to assess the estimator performance under combined longitudinal and lateral dynamic conditions.

For each maneuver and each tire, tread temperatures were measured immediately after the test using the tire pyrometer at three positions (inner, middle, and outer). The mean of these three measurements was taken as the representative tire temperature. It should be noted that, due to the ambient conditions during testing, tire operating temperatures were relatively low—ranging between 20 and 45 °C—whereas the optimal working temperature for this type of tire is approximately 60 °C. Data obtained with tire temperatures are available and are used to fit the model up to 65 °C. Nonetheless, these conditions are still considered representative for two reasons: first, this category of vehicle typically operates with relatively cold tires; and second, low-grip scenarios generally present the most challenging conditions for vehicle dynamics estimation and control.

3. Side Slip Angle Estimation Algorithm

Figure 2 describes the proposed vehicle slip angle estimation strategy, inspired by [2] but with tire temperature compensation. It is a comprehensive multi-sensor fusion architecture designed for the robust estimation of the vehicle sideslip angle (β). The methodology combines estimates from two parallel processing streams:

1. Kinematic Estimation Path: Utilizing sensor inputs such as lateral acceleration (a_y), yaw rate (r), and longitudinal velocity (V_x), the kinematic estimation block provides a responsive but drift-prone estimate ($\hat{\beta}_{kin}$). This estimate is subsequently processed by a pseudo-integration LP filter and gain block to mitigate integration drift.
2. Dynamic Estimation Path: The second path employs an Extended Kalman Filter (EKF) based on a dynamic vehicle model. The EKF combines direct sensor measurements ($a_y, a_x, r, \delta, T_{i,j}$), other relevant estimates (V_x, M_z), with the estimated lateral forces from the lateral force estimator ($F_{y,F}, F_{y,R}$) and the vertical loads from the vertical force estimator ($F_{z,i}$). The EKF produces a stable, model-based estimate of the sideslip angle ($\hat{\beta}_{EKF}$), which remains reliable even when kinematic data are unavailable or noisy.

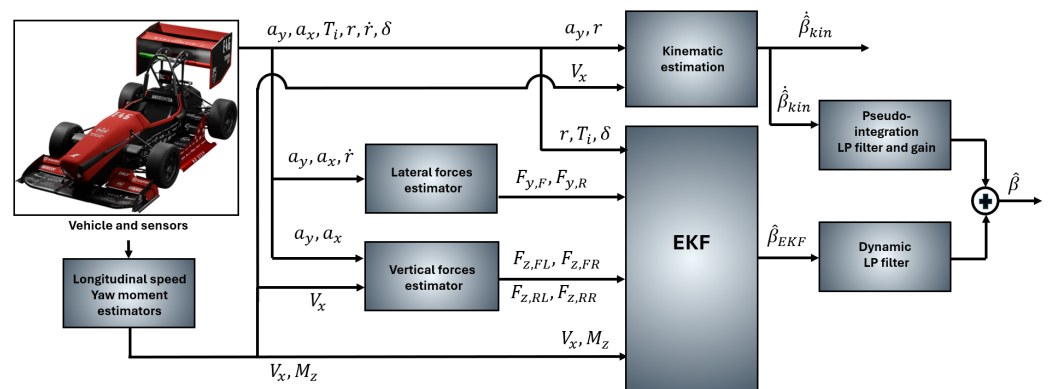


Figure 2. Estimator architecture: Longitudinal vehicle speed V_x is estimated by another model, as for M_z . Vertical and lateral forces estimator equation are reported respectively in Equations (8)–(11) and in Equations (13) and (14). Kinematic estimator equations are reported in (2) and (3). EKF internal model equations are reported in (4) and (5). The pseudo integrator and the Dynamic LP filters are presented in Equation (1).

The final, high-fidelity sideslip angle estimate ($\hat{\beta}$) is achieved by fusing (summing) the outputs of the two processed streams as in [2]. This architecture capitalizes on the short-term accuracy of the kinematic approach and the long-term stability of the dynamic EKF to produce an accurate and noise-resistant estimate across all driving conditions.

$$\hat{\beta} = \frac{1}{\tau_S + 1} \hat{\beta}_{EKF} + \frac{\tau}{\tau_S + 1} \hat{\beta}_{kin} \tag{1}$$

where τ is the time constant of the filters and is set to $\frac{10}{2\pi}$, following [2].

3.1. Kinematic Estimator

The kinematic estimator equations are reported in (2) and (3). The integration of the kinematic slip angle time derivative cannot be implemented in real world applications because it is affected by drifting induced by bias errors in the IMU [16,17].

$$a_{y,meas} = (\dot{\beta} + r) \cdot V_x - g \cdot \sin(\phi_r) \tag{2}$$

$$\hat{\beta}_{kin} = \int \dot{\beta} dt = \int \left(\frac{a_{y,meas} + g \cdot \phi_r}{V_x} - r \right) dt \tag{3}$$

The case-study vehicle exhibited a roll gradient such that the roll angle ϕ_r was extremely small. It was therefore reasonable to assume it to be zero in order to simplify the equations and measurements.

3.2. Model-Based Estimator

The model based estimator consists in an Extended Kalman Filter. The well known estimation algorithm is reported in appendix from [18]. The vehicle dynamics are represented by the following non-linear continuous-time differential equations:

$$\dot{\beta} = \frac{1}{m \cdot V_x} ((F_{y,FL} + F_{y,FR}) \cdot \cos(\delta) + F_{y,RL} + F_{y,RR}) - r \tag{4}$$

$$\dot{r} = \frac{1}{J_z} ((F_{y,FL} + F_{y,FR}) \cdot l_F \cdot \cos(\delta) - (F_{y,RL} + F_{y,RR}) \cdot l_R + (F_{y,FL} - F_{y,FR}) \cdot \sin(\delta) \cdot \frac{t}{2} + M_z) \tag{5}$$

with l_F and l_R as front and rear wheelbase, and t as the track of the vehicle equal for front and rear axles. M_z is the estimated yaw moment commanded by the torque vectoring and traction control installed on the vehicle and induced by ground longitudinal tire forces. Lateral forces are calculated from a Pacejka tire model $F_{y,ij}(\mu, F_{z,ij}, \alpha_{ij}, T_{ij})$ fed with vertical forces, tire temperature, and tire side slip angles. The latter are calculated as follows:

$$\alpha_{F,j} = \arctan\left(\frac{V_y + rx_j}{V_x - ry_j}\right) - \delta_j \tag{6}$$

$$\alpha_{R,j} = \arctan\left(\frac{V_y + rx_j}{V_x - ry_j}\right) \tag{7}$$

with V_x and V_y as the longitudinal and lateral component, respectively, of the vehicle speed, such that $V = \sqrt{V_x^2 + V_y^2}$. A detailed description of the tire model calibration process is provided in Section 3.4. Vertical forces are estimated as in Equations (8)–(11), starting from known vehicle parameters, vehicle speed, and accelerations through a rigid body, modeled as

$$F_{z,FL} = m \left(\frac{l_R}{l} g - \frac{h_{CoG}}{l} a_x \right) \left[\frac{1}{2} - \frac{h_{CoG} a_y}{t g} \right] + \frac{K_f \rho C_z V_x^2}{4} \tag{8}$$

$$F_{z,FR} = m \left(\frac{l_R}{l} g - \frac{h_{CoG}}{l} a_x \right) \left[\frac{1}{2} + \frac{h_{CoG} a_y}{t g} \right] + \frac{K_f \rho C_z V_x^2}{4} \tag{9}$$

$$F_{z,RL} = m \left(\frac{l_F}{l} g + \frac{h_{CoG}}{l} a_x \right) \left[\frac{1}{2} - \frac{h_{CoG} a_y}{t g} \right] + \frac{K_r \rho C_z V_x^2}{4} \tag{10}$$

$$F_{z,RR} = m \left(\frac{l_F}{l} g + \frac{h_{CoG}}{l} a_x \right) \left[\frac{1}{2} + \frac{h_{CoG} a_y}{t g} \right] + \frac{K_r \rho C_z V_x^2}{4} \tag{11}$$

The terms K_f, K_r are the aerodynamic repartition between front and rear axles, taking into account for theoad shift due to aerodynamic drag force as well. These are important when the vehicle has an important aerodynamic downforce and an uneven distribution of the generated forces: aerodynamic force balance has an effect on the vehicle balance (understeer or oversteer) that if not taken into account will induce an internal model mismatch with respect to reality. ρ is the air density, and C_z is the aerodynamic downforce coefficient. Yaw rate and lateral acceleration are measured via the IMU, and a steering sensor provides the steering angle.

Equations (4)–(11) represent the nominal model of the vehicle and can be condensed to the non-linear time-domain representation

$$\dot{\xi} = f(\xi, u, p), \tag{12}$$

with the state vector $\xi = [\beta, r]^T$, the yaw moment M_z as the manipulated input, the steering angle (δ) as the known disturbance input: $[\delta, M_z]^T \equiv u$. Vector $p = [v_x, a_x, a_y, T_{i,j}]^T$ umps the time-varying parameters:ongitudinal speed,ongitudinal acceleration, and lateral acceleration of the chassis and tire temperatures, respectively, all assumed as measured quantities available from the vehicle control unit (VCU). Hereinafter, the non-linear system (12) is referred to as the nominal model of the vehicle and used by the EKF to predict the vehicle dynamics.

Regarding the measurements used in the update phase of the EKF, the lateral forces ($F_{y,F}, F_{y,R}$), estimated from inertial measurements, are added as measured quantities [18,19]:

$$F_{y,F} = \frac{m a_y l_R + J_z \dot{r}_{meas}}{l_F + l_R} \tag{13}$$

$$F_{y,R} = \frac{m a_y l_F - J_z \dot{r}_{meas}}{l_F + l_R} \tag{14}$$

The measured yaw acceleration was obtained through real-time filtering using a Kalman filter specifically designed and tuned for derivative estimation. The measurement vector, used during the update phase of the estimator, is given by

$$z = [r \ F_{y,F} \ F_{y,R}]^T \tag{15}$$

with the measured $F_{y,F}$ and $F_{y,R}$ found with a bicycle model as in Equations (13) and (14).

The algorithm is implemented through the Euler discretization method with a sampling time of 0.01 s. The process and measurement covariance matrices are defined as follows and are assumed to be time-invariant:

$$Q = \begin{bmatrix} 1 \times 10^{-5} & 0 \\ 0 & 1 \times 10^{-3} \end{bmatrix}, \quad R = \begin{bmatrix} 1 \times 10^{-3} & 0 & 0 \\ 0 & 1 & 0 \\ 0 & 0 & 1 \end{bmatrix}.$$

The state vector ξ is always initialized at $\xi_0 = [0, 0]^T$ since for all the maneuvers the initial vehicle motion is in a straightline. The initial error covariance matrix P_0 is set equal to Q .

3.3. Internal Model Mismatches: The Need of an Adaptive Pacejka Model

The above-mentioned model is implemented with a given and validated Pacejka tire model, found with the tire in optimal condition regarding the temperatures, and it has already been rescaled to suit the track application in order to adapt the actual grip, cornering stiffness and saturation characteristics. Results for these implementations are shown in Figures 3 and 4, which report the kinematic estimation $\hat{\beta}_{kin}$, the EKF estimation $\hat{\beta}_{EKF}$, and the combined estimation $\hat{\beta}$ versus the measured slip angle duringow tire temperature maneuvers.

It can be noticed that the EKF contribution is stable but also fairly inaccurate since it overestimates the available grip and the vehicle slip angle. As a result, the combined estimation is not reliable enough, especially for a DLC maneuver in which the vehicle undergoes to an extreme understeer situation, exploiting the model of the tires in strong saturation.

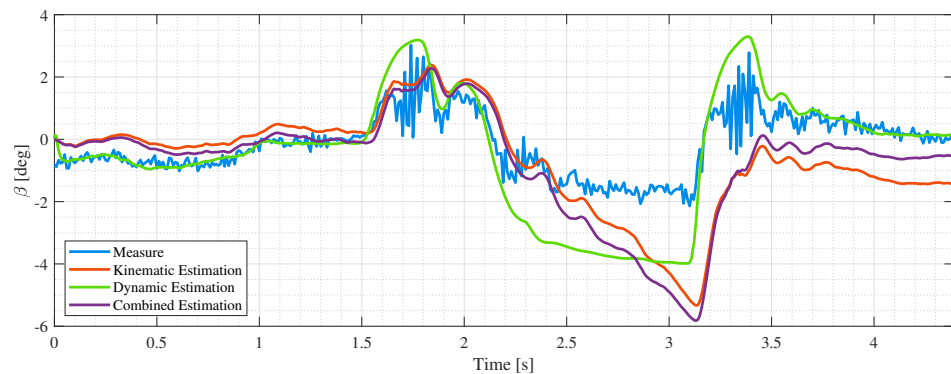


Figure 3. Slip angle estimation with a standard EKF and no tire model adaptation with respect to temperatures for a DLC maneuver with a tire temperatureover than 26 °C.

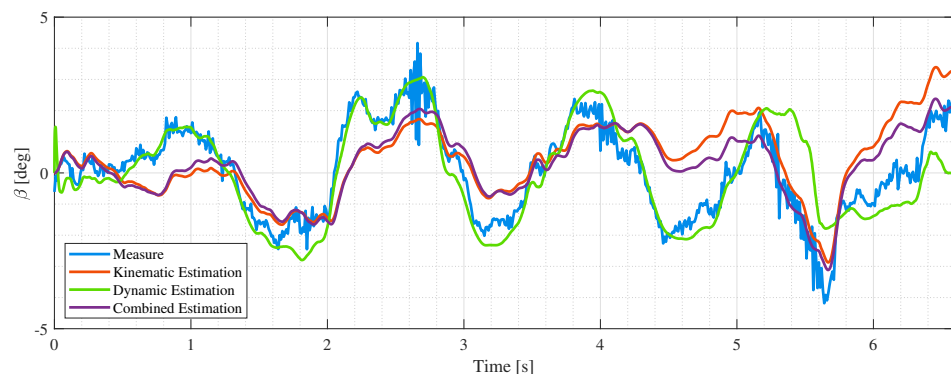


Figure 4. Slip angle estimation with a standard EKF and no tire model adaptation with respect to temperatures for a DLC maneuver with tire temperatureover than 32 °C.

The behavior of the vehicle changes dramatically when tire temperatures drop below the correct working window. This affects the estimation capability of the EKF due to mismatches between real vehicle and internal model. In Figure 5, we reported a comparison between two CRC maneuvers run with different tire temperatures.

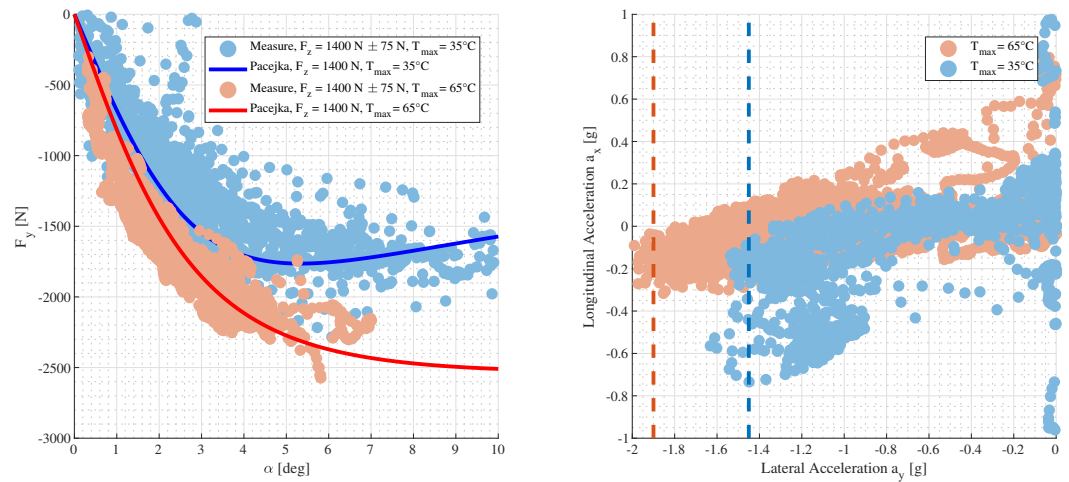


Figure 5. On the left side: F_y vs. α for two CRC runs at different tire temperatures, with the respective simulations held with a tuned Pacejka model (solid lines). On the right side, a GG plot of the same maneuvers. The red and blue dashed lines indicate the peak lateral acceleration values obtained after post-processing the measurements for CRC runs at 65°C and 35°C , respectively.

Experimental F_y points are obtained with Equation (14) and are associated with the maximum measured tire temperature between left and right, the hotter tire happens to be the external one since it is the more loaded. Solid lines are obtained with simulations of CRC maneuvers with a Pacejka model that tries to replicate the very same behavior as in the real world. Lateral and longitudinal accelerations are displayed in a GG diagram as suggested by [20] to highlight the different available peak lateral coefficient available: with hot tires, the vehicle can guarantee 1.9 g, while with cold tires, the maximum possible acceleration is below 1.5 g.

From the figures above, it is clear that it is not just a matter of tuning the grip scaling coefficients due to differences between the test rig and track adherence, because a single Pacejka model parameter set cannot interpolate correctly both the maneuvers. There is an important relationship with tire temperature since all other parameters like vehicle setup, air temperature, track temperature, and general condition are extremely similar, since the tests have been performed in the same session.

3.4. Adaptive Model Formulation and Parameters Fitting

The following adaptive Pacejka tire lateral model [21] has been chosen to have the temperature information to change the μ_y and saturation characteristic versus α .

$$dT = (T - T_0) / T_0 \tag{16}$$

$$C_y = p_{cy1} \cdot (1 + PTY1 \cdot dT + PTY2 \cdot dT^2) \tag{17}$$

$$dfz = (F_z - F_{z,0}) / (F_{z,0}) \tag{18}$$

$$m_{upy} = (pDy1 + pDy2 \cdot dfz)(1 - pDy3 \cdot \sin(\gamma)) \tag{19}$$

$$Dy = m_{upy} \cdot F_z (1 + PTY3 \cdot dT) \tag{20}$$

$$E_y = (pEy1 + pEy2 \cdot dfz)(1 - (pEy3 + pExy4 (\sin(\gamma))^2)) \tag{21}$$

$$K_{ya0} = F_{z,0} \cdot pky1 \cdot \sin(2 \cdot \text{atan}(F_z / (pky2 \cdot F_{z,0}))) \tag{22}$$

$$K_{ya} = K_{ya0} (1 - pky3 (\sin(\gamma))^2) \tag{23}$$

$$B_y = K_{ya} / (C_y \cdot Dy) \tag{24}$$

$$F_y = Dy \cdot \sin(Cy1 \cdot \text{atan}(By (1 - Ey) \cdot \alpha + Ey \cdot \text{atan}(By \cdot \alpha))) \tag{25}$$

where γ is the camber angle, $T_0 = 60 \text{ }^\circ\text{C}$, and $PTY1, PTY2, PTY3$ are the interpolated coefficients. The Jacobian matrices for the EKF are adapted with the new coefficients, not recomputed from scratch since temperature is not only measured by also slowly varying with respect to the states. An insight to the shown parameters can be found also in [22].

The above mentioned coefficients have been found with the a process that includes raw data filtering, Pacejka parameter fitting, and temperature-dependent coefficient fitting. During raw data filtering, axle lateral forces and tire sideslip angles are filtered through a moving average filter, with a sliding window of 0.1 s. Then Pacejka parameters $pcy1$ and $pDy1$ from a nominal temperature set are rescaled in order to minimize the squared error between the predicted axle force and the measured force. Subsequently, the obtained values of $pcy1$ and $pDy1$ are fitted as functions of the temperature at which they were identified yielding temperature-dependent coefficients, again minimizing the squared errors between the predicted Pacejka coefficient and the fitted Pacejka parameters. The result is shown in Figure 6.

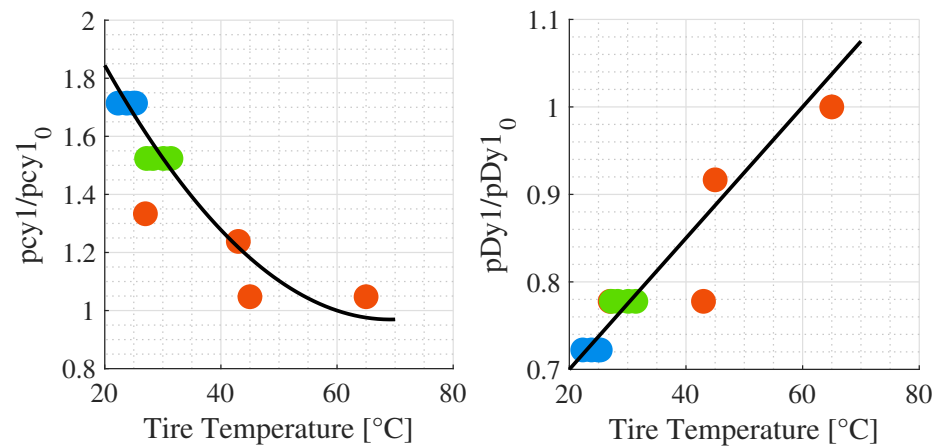


Figure 6. Interpolation of temperature-dependent coefficients. On the left, the relative change of $pcy1$ is reported; this parameter affects tire behavior at saturation operating conditions (high sideslip angles). On the right, the relative change of $pDy1$, which is directly related to μ_y . The maneuvers used for the interpolation are CRC, DLC 1, and slalom 1, represented in orange, blue, and green, respectively.

A parabolic approximation has been chosen for $pcy1$ behavior, while a linear model is used for $pDy1$. Each point represents a tire with its registered temperature, and points with the same color are associated with the same maneuver. To ensure the integrity of the results, the specific maneuvers utilized for tire model extraction were excluded from the validation dataset.

The registered tire temperatures are reported in Table 2. As mentioned, temperatures are measured for each tire at three different points at the end of the maneuver.

Table 2. Table with tire temperature for the analyzed maneuvers.

Tire	Registered Tire Temperatures [°C]						
	Fitting			Validation			
	DLC 1	Slalom 1	CRC	DLC 2	Slalom 2	Steering Sine Sweep	Track Lap
FL	24.8	30.1	56.2	24.9	42.0	20.4	46.5
FR	22.3	27.2	50.5	22.3	38.6	20.2	45.1
RL	24.5	31.4	64.8	25.3	42.8	20.6	49.0
RR	23.7	28.3	55.2	23.8	42.2	20.7	48.0

It must be pointed out that, for this work, temperatures are acquired during testing but are processed offline. Once the thermal model is defined through interpolation with standard maneuvers, tire temperature is artificially kept constant to the measured value from the end of the test with, as a “maneuver-wise” adaptation.

4. Experimental Results

The new and temperature adaptive estimations, represented with a solid line, are compared to the standard non-adaptive ones, represented with dashed lines.

4.1. Slalom and DLC: Pure Lateral Maneuvers

Figures 7 and 8 illustrate the results concerning mainly lateral maneuvers: DLC and slalom, respectively. The internal model of the EKF should be much more reliable, since it is based on a lateral only Pacejka and vehicle model, as it happens to be.

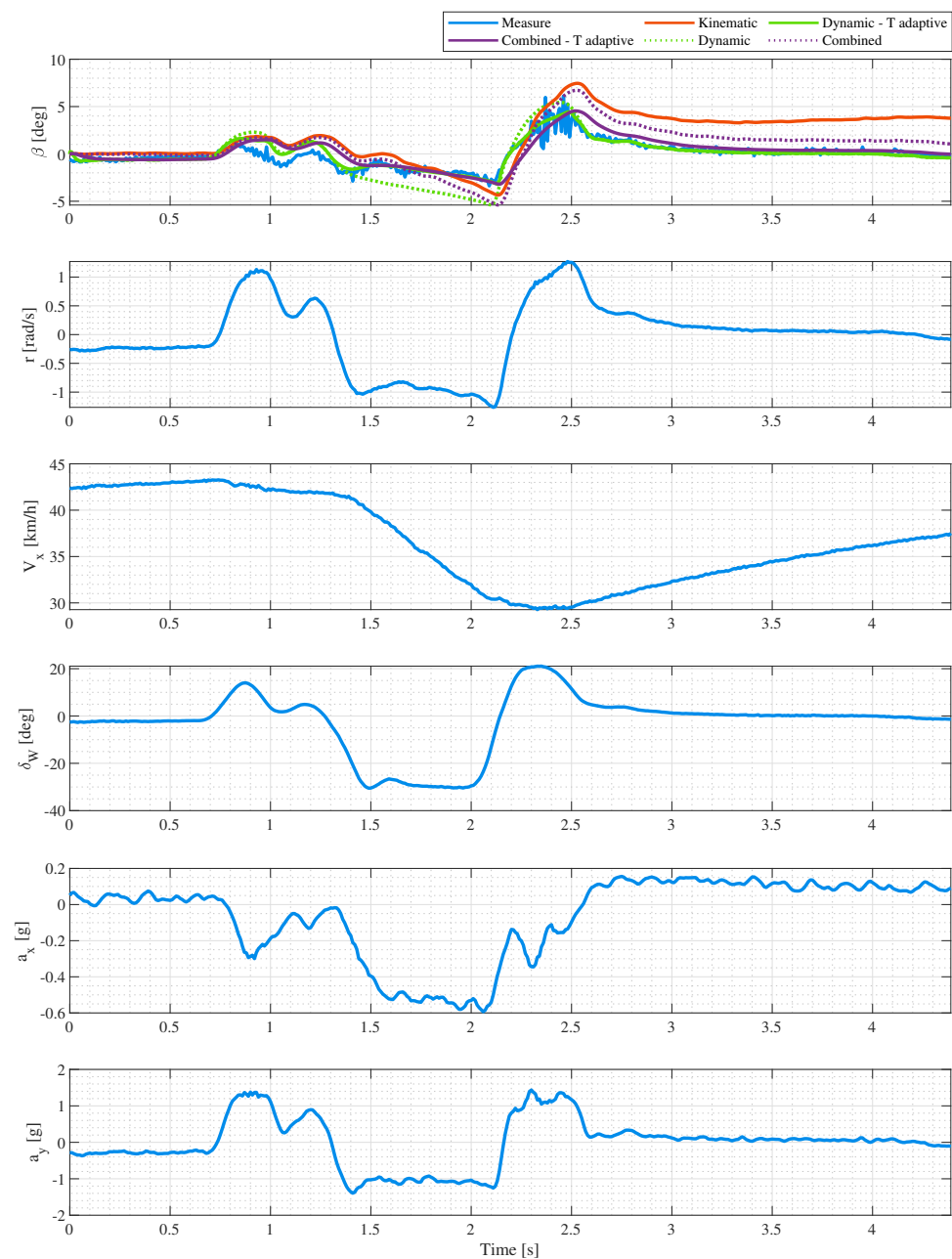


Figure 7. Slip angle estimation with an adaptive EKF for a DLC maneuver with tire temperature over than 25 °C.

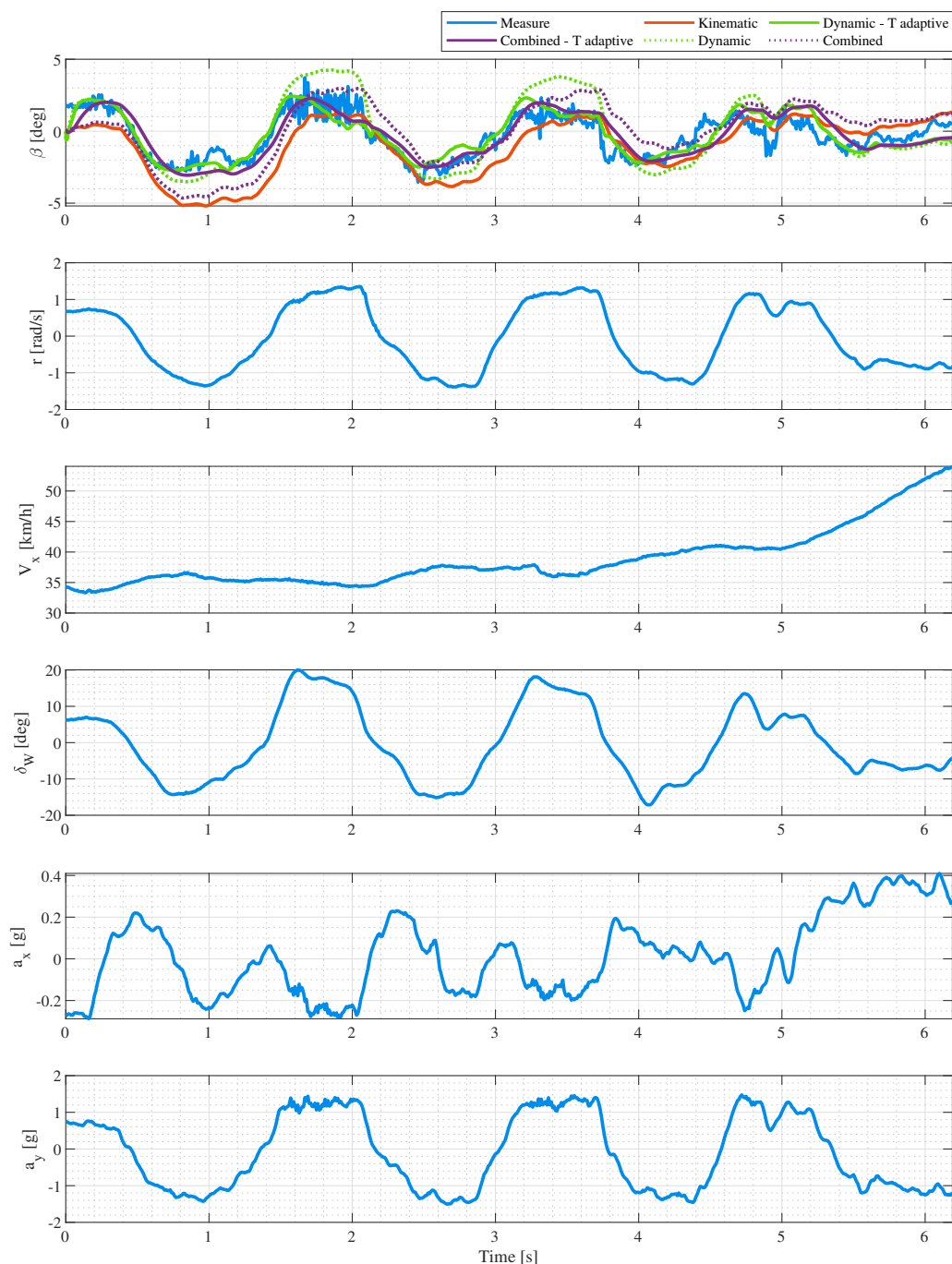


Figure 8. Slip angle estimation with an adaptive EKF for a slalom maneuver with tire temperature over than 43 °C.

4.2. Track Lap: Combined Longitudinal–Lateral

We have seen in previous figures that the EKF performs very well in lateral operation. The estimation algorithm must work in all possible situations, that is, for a tracklap when the vehicle is found to be at its adherence limit in a combined operation that includes braking while cornering (trail braking) and strong acceleration at the corner exit, as in Figure 9.

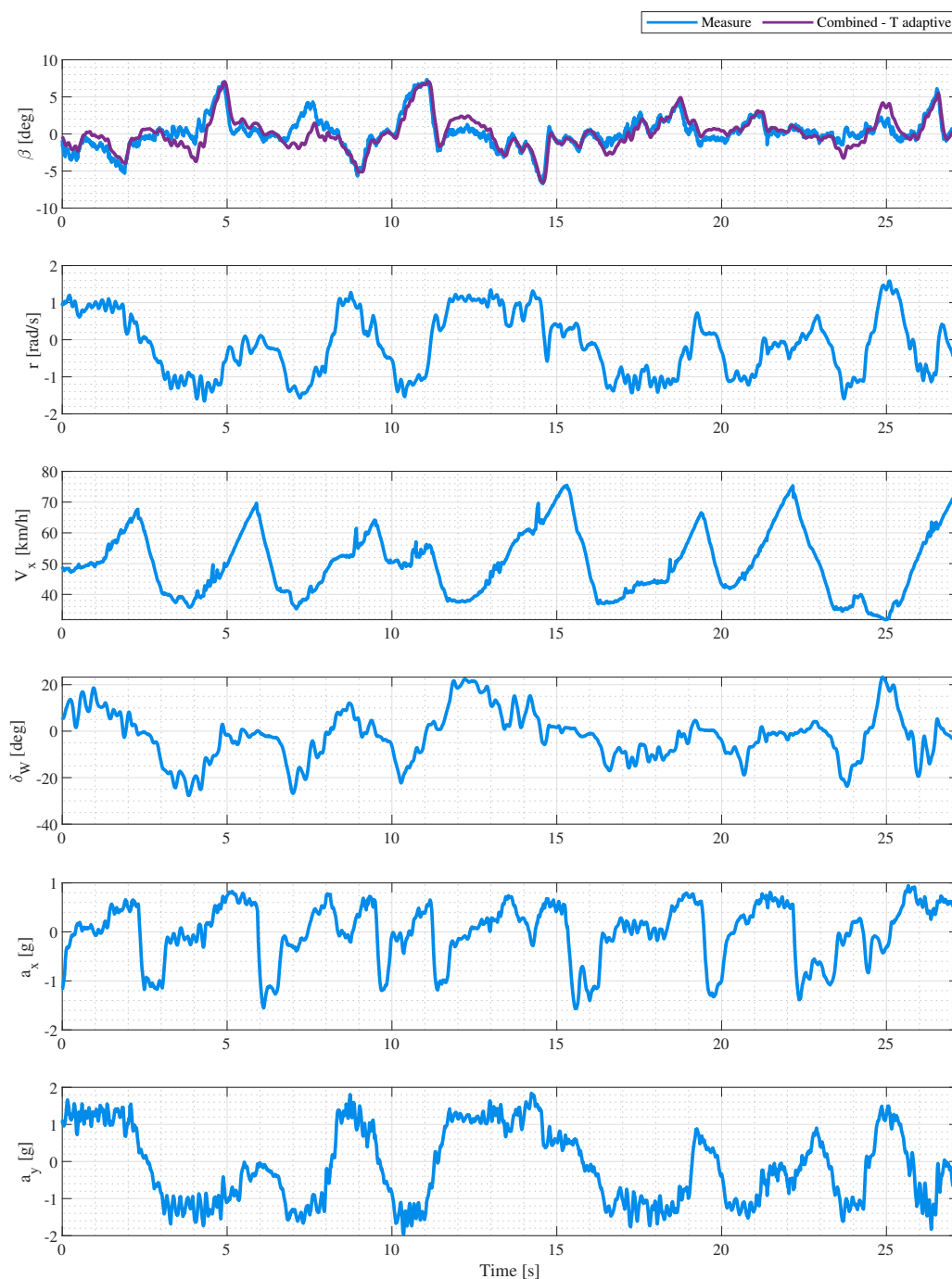


Figure 9. Slip angle estimation with an adaptive EKF for a slalom maneuver with tire temperature over than 50 °C.

It can be seen that, during a trackap, the combined estimation with the temperature adaptation is fairly reliable. We want to highlight that the tests are performed with a racing vehicle that usually exploits up to 8 deg of side slip angle. The estimator works perfectly while tracking the slip angle peaks, which are, for sure, the most delicate situations for both performance and safety. It is evident how, during a trackap, the vehicle experiences both lateral and longitudinal accelerations simultaneously, meaning that the tires are in combined longitudinal–lateral slip working points. Since the implementation presents a pure lateral Pacejka tire model, there is a limit in the performance of the EKF. The accuracy during acceleration and braking is not completely degraded, but is still guaranteed by the kinematic component $\hat{\beta}_{kin}$.

5. Discussion

The accuracy is now numerically assessed by looking at Maximum Absolute Error and RMS Error between each of the possible estimations and measurement. The errors are reported in the bar chart in Figure 10.

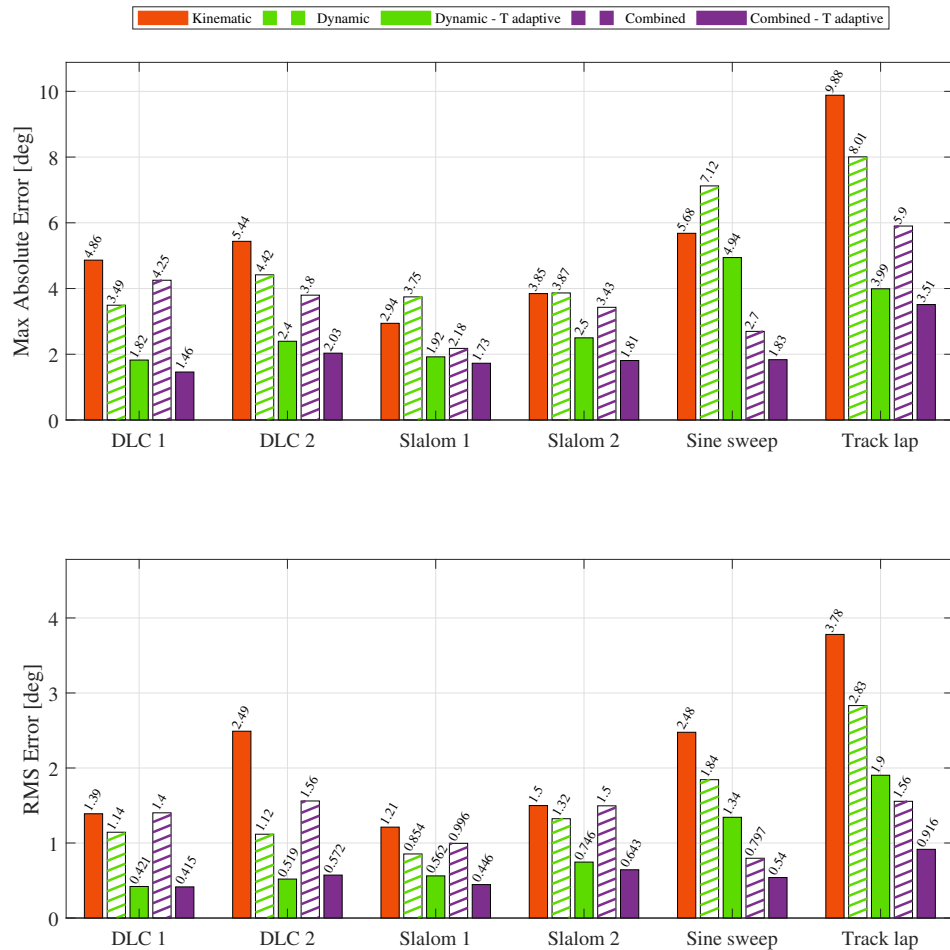


Figure 10. Bar chart representing the performance of the different contributions for the combined estimator tested on a representative maneuver set, comprehensive of DLC, slalom, steering sine sweep, and a trackap. A comparison is performed between the EKF with non-adaptive model and the tire-dependent one. The figure shows results for both fitting and validation maneuvers described in Table 2.

The experimental validation confirmed that incorporating tire temperature adaptation within the EKF framework leads to a consistent improvement in sideslip angle estimation accuracy. Comparative analysis among the kinematic, dynamic, and combined estimators highlights distinct performance characteristics depending on the driving condition.

For purely lateral maneuvers (such as the DLC and slalom tests), the temperature-adaptive EKF provided a more accurate representation of the tire behavior across different operating temperatures. The lateral force prediction improved markedly, reducing the overestimation of available grip that occurred with non-adaptive models. Consequently, the combined estimator (kinematic plus EKF) achieved the lowest RMS and maximum absolute errors in these tests, demonstrating the benefits of integrating tire thermal effects in scenarios dominated by lateral dynamics.

During mixed longitudinal–lateral maneuvers, such as the complete trackap, the adaptive EKF maintained good correlation with the measured slip angle, especially around peak sideslip conditions. However, residual discrepancies remained due to the simplified lateral-

only tire model and the absence of longitudinal slip coupling. These effects become significant during combined braking and acceleration phases, where the trade-off between longitudinal and lateral force capacity alters the tire's effective stiffness. The adaptive model partially mitigates these discrepancies by adjusting lateral stiffness with temperature, but cannot fully capture combined-slip behavior.

The statistical performance metrics shown in Figure 10 further substantiate these findings. The temperature-adaptive model consistently reduced RMS errors by up to 40–50% across all maneuvers. In particular, the DLC and slalom tests highlight a clear reduction in both RMS and maximum absolute errors when compared with the non-adaptive EKF, confirming the benefits of incorporating tire temperature effects into the estimation loop.

Nevertheless, Figure 10 also reveals that, in some cases, especially during pure lateral maneuvers, the combined estimator offers only marginal improvements over the adaptive dynamic EKF alone. This behavior suggests that, once the adaptive tire model compensates for most of the internal model mismatches, the contribution from the kinematic path becomes dominant in steady-state conditions.

Two additional aspects emerged as crucial for future development. First, tire temperature measurements obtained only at the end of each test are insufficient to fully capture the fast transient behavior observed during trackaps. As specified at the end of Section 3.4, the presented results are obtained through a “maneuvers-wise” tire temperature adaptation, not an online measurement and processing. Implementing real-time infrared temperature sensing would provide the necessary temporal resolution for online model adaptation. Second, the lack of longitudinal dynamics in the current EKF limits its capability under aggressive acceleration or braking, indicating the need for a combined-slip elliptical tire model and enhanced measurement fusion.

Overall, the proposed adaptive EKF demonstrates a strong balance between modeling accuracy and implementation practicality. It effectively bridges the gap between laboratory-calibrated tire models and real-world conditions, providing a robust foundation for high-performance vehicle state estimation and control.

6. Conclusions

This work presented a temperature-adaptive Extended Kalman Filter (EKF) for real-time sideslip angle estimation, validated experimentally on a Formula Student electric race car. The proposed approach integrates a temperature-dependent Pacejka tire model within a dual-track 3-DoF vehicle model, combining dynamic and kinematic estimation paths to enhance accuracy across a range of operating conditions.

The experimental results demonstrated that introducing tire temperature adaptation significantly improves estimation accuracy, particularly under low-grip and cold-tire scenarios. Quantitatively, the temperature-adaptive EKF reduced the RMS estimation error by up to 40–50% across the evaluated maneuvers compared to the non-adaptive baseline. The method showed the greatest benefits in pure lateral maneuvers (DLC and slalom), where tire temperature has a dominant influence on cornering stiffness. During full trackaps, the adaptive EKF maintained reliable estimation performance even in transient conditions involving combined longitudinal and lateral forces.

Despite these encouraging results, certain limitations remain. The current EKF formulation does not explicitly include longitudinal tire dynamics, and tire temperature is only sampled post-maneuver, which limits responsiveness during highly dynamic tests. Future developments will focus on integrating real-time infrared temperature sensing, combined-slip tire modeling, and state observers capable of online adaptation to tire wear and pressure variations.

Moreover, this methodology is easily transferable since the estimator is completely model-based. The relevant data for tire model fitting can be obtained with few sensors, some of which are already standard in the automotive industry. The needed tests can be performed in any dynamic platform as well as in a racetrack according to vehicle utilization and range of speed. Other Pacejka parameters can be introduced in order to rescale the actual peak gripevel of a new unknown racetrack without modifying the temperature response of the tire only.

Overall, the proposed framework provides an effective and practical compromise between model complexity, calibration effort, and estimation robustness. By relying solely on standard on-track tests to parametrize the adaptive tire model, the approach avoids expensive laboratory procedures while maintaining high accuracy—making it suitable for both motorsport applications and advanced vehicle dynamics control systems in broader automotive contexts.

Author Contributions: Conceptualization, R.M., L.M.C.M. and A.T.; methodology, A.M., R.M. and L.M.C.M.; software, A.M. and R.M.; validation, A.M.; writing—original draft preparation, A.M., R.M. and L.M.C.M.; writing—review and editing, L.M.C.M. and A.T.; supervision, A.T. All authors have read and agreed to the published version of the manuscript.

Funding: This research received no external funding.

Institutional Review Board Statement: Not applicable.

Informed Consent Statement: Not applicable.

Data Availability Statement: The original contributions presented in the study are included in the article, further inquiries can be directed to the corresponding author.

Acknowledgments: The authors gratefully acknowledge the LIM Mechatronics Lab, Politecnico di Torino (Turin, Italy), for providing the Correvit S-Motion non-contact optical sensor (Kistler) employed during the experimental campaign.

Conflicts of Interest: The authors declare no conflicts of interest.

References

1. Rajamani, R. *Vehicle Dynamics and Control*; Springer: New York, NY, USA, 2006.
2. Piyabongkarn, D.; Rajamani, R.; Grogg, J.A.; Lew, J.Y. Development and Experimental Evaluation of a Slip Angle Estimator for Vehicle Stability Control. *IEEE Trans. Control Syst. Technol.* **2009**, *17*, 78–88. [[CrossRef](#)]
3. Ryu, J.; Gerdes, J.C. Integrating inertial sensors with GPS for vehicle dynamics control. *J. Dyn. Syst. Meas. Control* **2004**, *126*, 243–254. [[CrossRef](#)]
4. Goodwin, G.C.; Doná, J.A.; Seron, M.M. *Constrained Control and Estimation: An Optimisation Approach*; Springer Science & Business Media: London, UK, 2006.
5. Simon, D. *Optimal state estimation: Kalman, H Infinity, and Nonlinear Approaches*; John Wiley & Sons: Hoboken, NJ, USA, 2006.
6. Singh, K.B. Vehicle Sideslip Angle Estimation Based on Tire Model Adaptation. *Electronics* **2019**, *8*, 199. [[CrossRef](#)]
7. Nishio, A.; Tozu, K.; Yamaguchi, H.; Asano, K.; Amano, Y. Development of Vehicle Stability Control System Based on Vehicle Sideslip Angle Estimation. *SAE Trans.* **2001**, *110*, 115–122.
8. Jonathan, Y.M.G.; Thompson, M.; Dallas, J.; Balachandran, A. Beyond the stable handling limits: Nonlinear model predictive control for highly transient autonomous drifting. *Int. J. Veh. Mech. Mobil.* **2024**, *62*, 2590–2613.
9. Kobayashi, T.; Weber, T.P.; Gerdes, J.C. Trajectory planning using tire thermodynamics for automated drifting. In Proceedings of the 2024 IEEE Intelligent Vehicles Symposium (IV), Jeju Island, Republic of Korea, 2–5 June 2024; IEEE: Piscataway, NJ, USA, 2024; pp. 2103–2109.
10. Chindamo, D.; Lenzo, B.; Amodeo, S.; Dalla Via, L.; Sakhnevych, A. On the Vehicle Sideslip Angle Estimation: A Literature Review of Methods, Models, and Innovations. *Appl. Sci.* **2018**, *8*, 355. [[CrossRef](#)]
11. Ahangarnejad, M.; Ordys, A.; Askari, M.; O'Neill, E.; Iravani, P. ADAP-TYRE DEKF Filtering for Vehicle State Estimation Based on Tyre Parameter Adaptation. *Int. J. Veh. Dyn.* **2016**, *2*, 330–350. [[CrossRef](#)]

12. Naets, B.; Van Aalst, H.; Desmet, W. Design and Experimental Validation of a Stable Two-Stage Estimator for Automotive Sideslip Angle and Tyre Parameters. *IEEE Trans. Veh. Technol.* **2017**, *66*, 4573–4586. [CrossRef]
13. SBG Systems. Ellipse Series—Hardware Manual. Available online: <https://support.sbg-systems.com/sc/el/files/latest/102924736/102924734/1/1720519483812/Ellipse+3+-+Hardware+Manual.pdf> (accessed on 1 July 2025) .
14. Kistler. Correvit S-Motion. Available online: https://kistler.cdn.celum.cloud/SAPCommerce_Download_original/003-395e.pdf (accessed on 1 July 2025) .
15. RLS. RM08. Available online: <https://www.rls.si/eng/rm08-super-small-non-contact-rotary-encoder> (accessed on 1 July 2025) .
16. Selmanaj, D.; Corno, M.; Panzani, G.; Savaresi, S.M. Vehicle sideslip estimation: A kinematic based approach. *Control Eng. Pract.* **2017**, *67*, 1–12. [CrossRef]
17. Tseng, H.; Madau, D.; Ashrafi, B.; Brown, T.; Recker, D. Technical challenges in the development of vehicle stability control system. In Proceedings of the 1999 IEEE International Conference on Control Applications (Cat. No.99CH36328), Kohala Coast, HI, USA, 22–27 August 1999; Volume 2, pp. 1660–1666. [CrossRef]
18. Molina, L.M.C.; Manca, R.; Hegde, S.; Amati, N.; Tonoli, A. Predictive handling limits monitoring and agility improvement with torque vectoring on a rear in-wheel drive electric vehicle. *Veh. Syst. Dyn.* **2024**, *62*, 2185–2209. [CrossRef]
19. Cheli, F.; Sabbioni, E.; Pesce, M.; Melzi, S. A methodology for vehicle sideslip angle identification: Comparison with experimental data. *Veh. Syst. Dyn.* **2007**, *45*, 549–563. [CrossRef]
20. Milliken, W.F.; Milliken, D.L.; Metz, L.D. *Race Car Vehicle Dynamics*; SAE International: Warrendale, PA, USA, 1994.
21. Pacejka, H.B. *Tyre and Vehicle Dynamics*, 3rd ed.; SAE International: Warrendale, PA, USA; Butterworth Heinemann: Oxford, UK, 2012.
22. Genta, G.; Morello, L. *The Automotive Chassis: Volume 1: Components Design*; Springer: Dordrecht, The Netherlands, 2009; Chapter 2, pp. 53–132.

Disclaimer/Publisher’s Note: The statements, opinions and data contained in all publications are solely those of the individual author(s) and contributor(s) and not of MDPI and/or the editor(s). MDPI and/or the editor(s) disclaim responsibility for any injury to people or property resulting from any ideas, methods, instructions or products referred to in the content.